ACS NANO
Cite This: ACS Nano XXXX, XXX, XXX–XXX
www.acsnano.org

ARTICLE

Single-Molecule Discrimination of Labeled DNAs and Polypeptides Using Photoluminescent-Free TiO_2 Nanopores

Rui Wang,[†,#] Tal Gilboa,[†,#] Jiaxi Song,[‡] Diana Huttner,[†] Mark W. Grinstaff,[*,‡] and Amit Meller[*,†,‡]

[†]Department of Biomedical Engineering, Technion—IIT, Haifa, 32000, Israel
[‡]Department of Biomedical Engineering, Boston University, Boston, Massachusetts 02215, United States

Supporting Information

ABSTRACT: **Multicolor fluorescence substantially expands the sensing capabilities of nanopores by complementing or substituting the resistive pulsing signals. However, to date single-fluorophore detection in multiple color channels has proven to be challenging primarily due to high photoluminescence (PL) emanating from the silicon nitride (SiN_x) membrane. We hypothesize that the high bandgap of titanium oxide (TiO_2) would eliminate the PL background when used as a substrate for a nanopore, and hence enable individual fluorophore sensing during the fast passage of biomolecules through the pore. Herein, we introduce a method for fabricating locally supported, free-standing, TiO_2 membranes, in which solid-state nanopores can be readily drilled. These devices produce essentially no PL in the blue-to-red visible spectral range, even when excited by multiple lasers simultaneously. At the same time, the TiO_2 nanopores exhibit low electrical noise comparable with standard SiN_x devices. Importantly, the optical signal-to-background ratio (SBR) in single-molecule sensing is improved by an order of magnitude, enabling the differentiation among labeled DNA molecules of similar length based solely on their labeling scheme. Finally, the increased SBR of the TiO_2 devices allows detection of single fluorophores conjugated to the lysine or cysteine residues of short polypeptides, thus introducing the possibility for optical based peptide/protein discrimination in nanopores.**

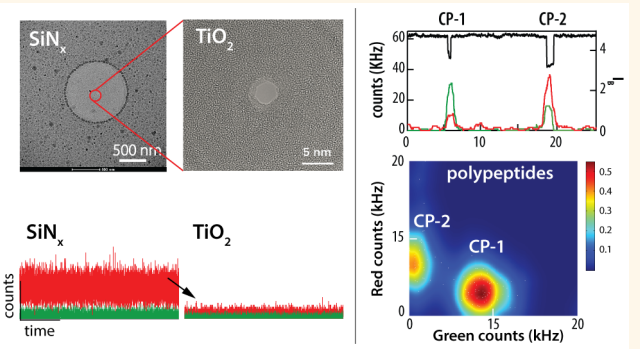

KEYWORDS: *solid-state nanopore, electro-optical sensing, titanium dioxide, single-molecule sensing, polypeptide identification*

Solid-state nanopores have emerged as extremely versatile single-molecule biosensors for biomolecules, such as DNAs and RNAs.[1−3] In a nanopore system, the applied electrophoretic force threads the electrically charged biopolymers through a nanoscale constriction, forcing the biopolymers to linearize and translocate across an insulating membrane.[4] The same electrical voltage that mobilizes the biomolecule generates an ionic current through the nanopore, which is temporally altered by the molecule's cross-section, and/or local structure during its passage. This sensing principle, commonly referred to as "resistive pulsing" is employed for genotyping and DNA sequencing as well as for the study of DNA−protein interactions.[5−11] Building on the learnings from nucleic acid detection, nanopores are now being used to detect proteins, demonstrating that ion current traces contain information about protein size and structure.[12−17] However, to date, the challenge of deconvolving the electrical ion current trace to discriminate among polypeptides remains unresolved.

The sensing capabilities of nanopores employing resistive pulsing are significantly enhanced with the addition of a second independent means of detection.[18,19] One example is optical sensing, which is used for DNA barcode discrimination, mapping of epigenetic modifications, and DNA length discrimination.[20−24] Additionally, as proteins contain modifiable lysine and cysteine residues, which can be respectively tagged with fluorescent dyes, the opportunity exists to discriminate among proteins,[25] even in cases in which their electrical current fingerprints are indistinguishable. However, despite growing interests in single-molecule protein identification,[26] a method that can scan a linearized peptide or protein while sensing *individual fluorophores* has not been reported due to the strict requirements for extremely low optical background and high temporal resolution.

Received: September 14, 2018
Accepted: October 29, 2018
Published: October 29, 2018

DOI: 10.1021/acsnano.8b07055
ACS Nano XXXX, XXX, XXX–XXX

Free-standing silicon nitride (SiN_x), is widely used to form low-stress thin films in solid-state nanopores due to its low capacitance and high resistance. However, SiN_x produces significant photoluminescence (PL) when illuminated by blue-green lasers, typically used for single-molecule fluorescence detection thereby hindering multicolor sensing.[21,22] In contrast, the large band gap of titanium oxide (TiO_2, 3.0 eV for rutile and 3.2 eV for anatase) minimizes its sensitivity to visible light in the blue to red visible spectrum range, therefore potentially reducing its PL emission.[27−29] A thin layer of TiO_2 has been previously applied on top of a graphene membrane, as well as on top of SiN_x to improve the electrical and optical performance, respectively, while permitting the formation of water-filled nanopores.[30,31] Accordingly, we postulate that amorphous, free-standing TiO_2 membranes will improve the signal to background ratio (SBR) in optical sensing remarkably by reducing the PL background from the nanopore membrane, making it a high quality material for optical sensing in a solid-state nanopore.

To test this hypothesis, we developed a method for the fabrication of locally supported, free-standing thin TiO_2 membranes, in which solid-state nanopores are drilled either by focused electron beam in high-resolution transmission electron microscopy (HR-TEM)[32,33] or by a controlled dielectric breakdown (CDB) process.[34] The TiO_2 membranes are easily drilled and are readily wettable. Remarkably, the TiO_2 membranes produce negligible PL that is an order of magnitude lower than that of a free-standing SiN_x of the same thickness at the typical light intensities and wavelengths used for single-molecule sensing, while preserving low electrical noise properties. The highly reproducible and parallel fabrication of the free-standing TiO_2 nanopores allowed us to observe electro-optical signals from individually labeled DNA samples, as well as two colors photon bursts from a short polypeptide, conjugated with different fluorophores at the cysteine or lysine residues respectively, during their translocation through a ∼3 nm pore.

RESULTS AND DISCUSSION

Electrical Characterization of Free-Standing TiO_2 Nanopores. In order to manufacture free-standing TiO_2 nanopores in thin membranes of a controllable thickness, we describe a wafer-scale fabrication method, utilizing an in-house photolithographic process and a desktop atomic layer deposition (ALD) process. Our method is summarized in the Methods section and Figure 1a. A detailed step-by-step description is also provided in the Supporting Information (Figure S1). Briefly, the free-standing TiO_2 membrane is formed at the center of a thicker SiN_x membrane serving two functional roles: (1) to mechanically support the local ultrathin (<10 nm) free-standing TiO_2 membrane, and (2) to facilitate optical localization of the nanopore, while positioning the pore at the microscope focal zone.

Figure 1b (left) shows white light image in reflection mode of the SiN_x/TiO_2 membrane, taken from the front side. The thinner, free-standing TiO_2 membrane is seen as a darker spot in the membrane. Figure 1b (right-hand panels) show transmission electron microscopy (TEM) images at low and high magnifications of the membrane. The free-standing TiO_2 membrane is well-defined by a distinct circle formed at the SiN_x/TiO_2 interface. The high magnification TEM image displays a 4 nm nanopore that was formed by a focused TEM *e*-beam in the TiO_2 membrane. In addition to TEM drilling, we could readily use CDB to form nanopores. As can be seen in Figure 1c, and in agreement with previous findings, the nanopore forms preferably at the thinnest region of the membrane.[34] This observation is corroborated by wide-field fluorescence microscopy using Ca^{2+} activated fluorophores. Upon applying a +300 mV bias, a bright fluorescent spot appears at the nanopore location (overlapping with the thin region location, imaged using white light), where Ca^{2+} ions are drawn through the nanopore and react with the Ca^{2+} indicator dyes (Fluo-4, Thermo Fisher) (left panel). The fluorescent spot immediately disappears when an opposite voltage bias is applied (right panel).

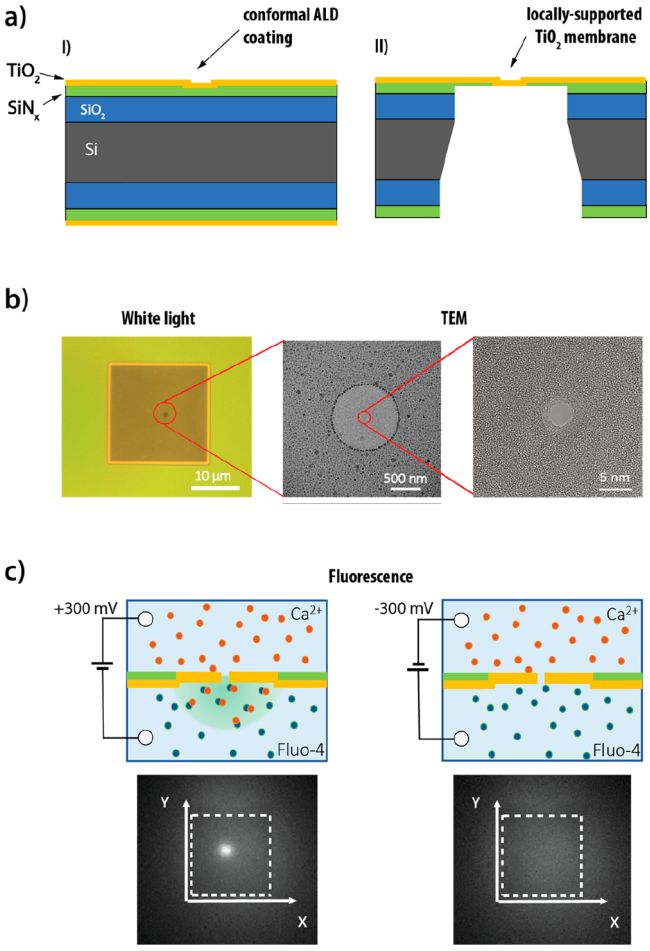

Figure 1. Fabrication and characterization of the TiO_2 nanopore sensor. (a) Wafer-scale fabrication of the TiO_2 devices (see Supporting Information, sections S1 and S2 for detailed description). A thin region is created in the SiN_x by selective RIE, followed by ALD deposition of TiO_2 (i). KOH and RIE are then used to expose the free-standing SiN_x/TiO_2 membrane, containing a freely suspended TiO_2 circular region (ii). Nanopores are fabricated using CDB or TEM. (b) (Left panel) reflected white light image of a 22 μm SiN_x/TiO_2 membrane. The thin region is visible as a dark spot; (middle panel) TEM image of the freely suspended TiO_2 thin region, and its interface with the SiN_x/TiO_2 membrane; (right panel) a high-magnification TEM image of 4 nm TiO_2 nanopore drilled by TEM. (c) Wide field illumination images of the entire membrane using 488 nm laser. Calcium (Ca^{2+}) activated fluorophores are used for verifying the creation and position of a nanopore drilled by CDB. At 300 mV calcium is passing through the pore, and binding Fluo-4, resulting in a fluorescence spot in the thin region (left panel). The spot disappears when the bias is reversed to −300 mV (right panel). The membrane position is outlined by white dashed line.

DOI: 10.1021/acsnano.8b07055
ACS Nano XXXX, XXX, XXX−XXX

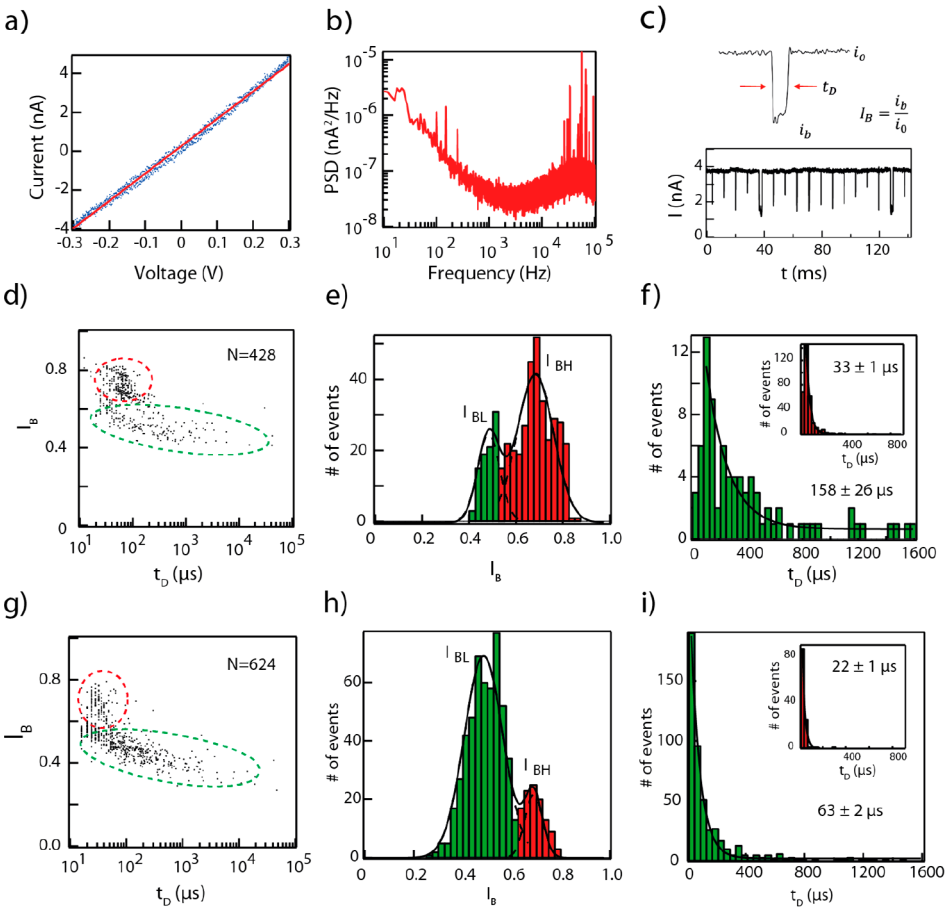

Figure 2. Electrical noise characterization and DNA translocation in free-standing TiO_2 nanopores. (a) Measured current−voltage (I−V) curve of a TiO_2 nanopore. The red line represents a linear fit to the data giving conductance of 14.08 ± 0.03 nS. (b) Power spectral density (PSD) of TiO_2 nanopore current measured at 300 mV and filtered at 100 kHz. (c) Concatenated DNA translocation events measured at 300 mV. Zoomed-in event and the parameters used for analysis are shown in the upper panel. (d) Scatter plot (I_B *versus* t_D) of 428 events measured at 200 mV. Two distinct populations are interpreted as translocation events (green dashed oval) and collision events (red dashed oval). (e) I_B histogram of all the events measured at 200 mV. The data is fitted by a double Gaussian model to yield the lower peak I_{BL}= 0.48 ± 0.01, and the higher peak I_{BH} = 0.68 ± 0.01 (green and red, respectively). f) Dwell time histogram of the translocation events (green column) and the collision events (red column, insert) at 200 mV. Time constants (τ) are extracted by tail fitting with exponential function. (g−i) Scatter plot, I_B histogram (I_{BL} = 0.49 ± 0.01, I_{BH} = 0.69 ± 0.01), and a dwell time histogram of 624 events measured at 400 mV.

We evaluated the functionality of the free-standing TiO_2 nanopores, by performing extensive electrical characterizations and DNA translocation experiments. After fabrication, the chip was thoroughly cleaned and glued to a matching PTFE cell, which can be accessed optically for high resolution epi-fluorescence sensing (see Methods). Prior to performing the biopolymer translocation experiments, the current−voltage curve and power spectral density (PSD) were measured, at 100 kHz bandwidth. Figure 2 panels a and b show a symmetrical and linear I−V curve with conductance (G) of 14.08 ± 0.03 nS. This result agrees with an estimated membrane thickness (l) of 15 nm and nanopore diameter (d) of 3.7 nm according to $G = \sigma\left[\frac{4l}{\pi d^2} + \frac{1}{d}\right]^{-1}$, where the bulk conductance is σ = 10.5 S m^{-1} at 23 °C.[35] The noise spectra exhibit the typical $1/f$ contribution at low frequencies and ~f^2 rise above ~5 kHz, with similar values to low-noise SiN_x nanopores.[36,37] Next, we added ~0.5 nM of a 5054-bp double stranded DNA solution prepared in house (see Supporting Information Figure S4) to the negatively biased chamber, and recorded the ion current as a function of time at 200 mV, 300 mV, and 400 mV bias. Figure 2c displays representative concatenated events at 300 mV. Each event is characterized by its open-pore current (i_o), blocked-pore current (i_b), and dwell time (t_D). The fractional blockade current is calculated as $I_B = i_b/i_o$ allowing us to directly compare experiments with different voltages since $i_o \propto V$, as shown in Figure 2a. Figure 2d−f and Figure 2g−i show the DNA translocation results for 200 mV and 400 mV, respectively. Figure 2d and 2g present the scatter plot of I_B *versus* t_D. As observed previously for nanopores of similar diameter and DNA length, the translocation events fall into two distinct populations: (1) short, low-amplitude and weakly voltage-dependent events attributed to DNA molecule colliding, but not translocating through the nanopore (red dashed oval); and (2) longer, deep amplitude and strongly voltage-dependent events attributed to full translocation of the DNA molecules through the nanopores (green dashed circle).[38,39]

Figure 2 panels e and h show the I_B histogram of all the events at 200 mV and 400 mV, respectively. As seen on the scatter plots, we discern two peaks: a higher I_B peaks (low amplitude events, I_{BH}) attributed to brief DNA collisions with the nanopore, and lower I_B peaks (high amplitude events, I_{BL}) attributed to translocations. The histograms are fitted using a double-Gaussian model, from which the events are classified into either

DOI: 10.1021/acsnano.8b07055
ACS Nano XXXX, XXX, XXX−XXX

collision (red) or translocation (green). To characterize collision and translocation events separately, a threshold is selected to remove >97% collision events from translocation events. The threshold (I_{BT}) is defined as $I_{BH}-2\sigma_H$, where σ_H is the standard deviation of I_{BH} Gaussian. Events with I_B smaller or larger than I_{BT} are treated as "translocation events" (green histogram) or "collision events" (red histogram), respectively. Notably, the translocation peak (I_{BL}) values remained constant in the two experiments 0.48 ± 0.01 at 200 mV and 0.49 ± 0.01 at 400 mV. Additionally, the percentage of translocation event of the total number of events increases with voltage (21% at 200 mV to 82% at 400 mV). This result further supports our interpretation of the low amplitude (green) events as translocations, since higher electrical-field lowers the energy barrier associated with DNA threading into the nanopore and its linearization. These values are used to further characterize the nanopore diameter by approximating the fractional blockade current by $I_{BL} = 1 - \left(\frac{a}{d}\right)^2$ indicating the nanopore diameter is ~3.1 nm, where a = 2.2 nm is the DNA diameter.[38] This result is close to our approximation of the pore diameter based on the open pore conductance, likely suggesting that the local TiO_2 thickness is slightly thinner than the ellipsometric measurement.

Figure 2 panels f and i present the dwell time histograms for the low amplitude events (green) and higher amplitude events (red) in inserts. The time constants, obtained by tail fitting of the histograms with exponential function, are 158 ± 26 μs at 200 mV and 63 ± 2 μs at 400 mV for the green events, and 33 ± 1 μs at 200 mV and 22 ± 1 μs at 400 mV for the red events. The strong reduction in the dwell time at higher voltage is consistent with our interpretation of DNA translocation events, whereas the rest of the event (red groups) dwell times are weakly dependent on voltage and may correspond to DNA collisions.

Photoluminescence (PL) Properties of the Free-Standing TiO_2 Membranes. For our studies, PL is more important than reflectance since the former heavily determines the SBR for single-fluorophore sensing, while the latter can be effectively excluded using cutoff optical filters. To that end, two nearly identical chips were fabricated possessing either a free-standing 15 nm thick SiN_x or TiO_2 membrane as schematically shown in Figure 3a. The membrane thicknesses were confirmed by ellipsometry (Film Sense, FS-1). Since the PL levels of the thin films (in water solution) are extremely small, we constructed a custom confocal apparatus, described schematically in the Supporting Information Figure S3, which includes three laser sources (532, 561, and 640 nm), a high numerical aperture water immersion microscope objective (×63/1.15), and the ability to either acquire the signal using a spectrometer (Ocean Optics) or by single photon counting Avalanche photo diodes (APDs) at two spectrally separated bands at 650 nm.

We first measured the characteristic spectral emission when illuminating using a green laser (532 nm). The two chips were carefully positioned at the laser focal point using an $X-Y-Z$ nanopositioner to ensure accurate placement at the peak reflected intensity. Note that integration time of ~5 s was required to obtain the full spectra. Our results (Figure 3a), show that both materials exhibit a broad PL emission distributed in the range of 600–900 nm, with a peak around 700 nm. Noticeably, however, the total TiO_2 PL intensity (estimated by the area under the corresponding spectra) appears to be roughly an order of magnitude smaller than the SiN_x PL. Typical photon emission time traces of the Green channel (570–650 nm) and the Red channel (650–750 nm), measured at 150 μW laser

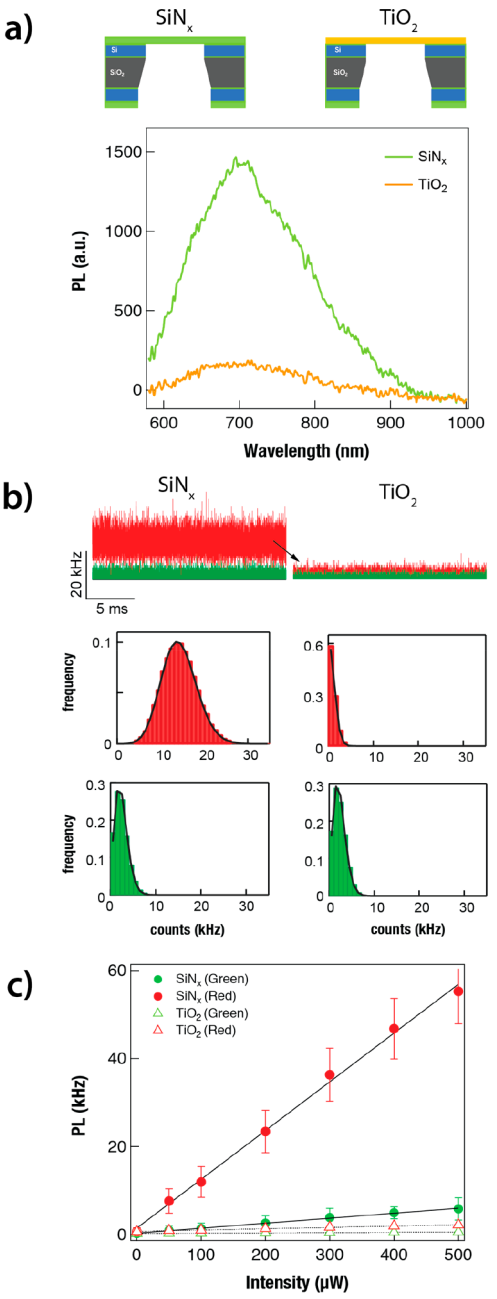

Figure 3. PL characterization of free-standing SiN_x and TiO_2 membranes. (a) Top panel shows the structures of free-standing SiN_x and TiO_2 membranes with a thickness of 15 nm. Bottom panel presents PL intensity spectral emission of SiN_x and TiO_2 membranes when illuminated with a 532 nm laser. SiN_x emits higher PL intensity than TiO_2 in large wavelength bandwidth. (b) PL intensity in the green channel (green color) and the red channel (red color) when illuminated with 561 and 640 nm lasers of 150 μW each. The top panel shows the PL intensity time traces. The bottom panel presents the histogram of the PL emission in the red and the green channels, which are fitted with Poisson distributions. Fittings values: Λ_1 = 1.81 ± 0.03, Λ_2 = 0.52 ± 0.01, Λ_3 = 1.85 ± 0.02, Λ_4 = 13.78 ± 0.06, for the TiO_2 green channel, the TiO_2 red channel, the SiN_x green channel, and the SiN_x red channel, respectively. (c) PL emission in the two APD channels when the membranes are illuminated with a 561 nm laser as a function of the laser intensity (additional data is provided in the SI). The four traces show a linear dependency of the PL on the laser intensity, while the TiO_2 PL intensity increase per μW is 10-fold lower than in the SiN_x device.

DOI: 10.1021/acsnano.8b07055
ACS Nano XXXX, XXX, XXX–XXX

intensity using the APD single-photon counting modules, are shown in Figure 3b for the SiN_x and TiO_2 membranes. Two salient features are apparent: first, the red-channel background PL of the SiN_x membrane is significantly increased as compared to the corresponding TiO_2 background PL. Second, the green channel of the background PL of the SiN_x membrane is only slightly larger than the corresponding TiO_2 background PL. These signals are further quantified by evaluating the photon intensity histograms shown in the lower panels of Figure 3b. In all cases, the photon histograms can be fitted well by Poisson functions as indicated in the figure caption.

Figure 3c displays the PL in the two fluorescence channels when excited by the yellow laser (561 nm) as a function of laser intensity for the SiN_x (solid circles) and TiO_2 (empty triangles) devices. In all cases, a linear dependency of the PL intensity on laser power is observed, as expected. Importantly, however, there is >10-fold difference in the PL background intensity per μW of laser intensity between the SiN_x and TiO_2 devices. Finally, linear-regression fits to the red data channel give 111 ± 3 Hz/μW and 3.0 ± 0.1 Hz/μW for the SiN_x and TiO_2 devices, respectively, which is an improvement by nearly a factor of 40.

Electro-Optical Discrimination among Two-Colors Labeled DNA Molecules. The highly reduced PL background of the TiO_2 membrane, presented in Figure 3, is noteworthy and suggests that an improved SBR for single-molecule fluorescence measurements will be obtained during the translocation of a labeled biomolecule through the nanopore. Importantly, the measurement of photon bursts emanating from fluorophore-conjugated biomolecules during their fast translocation through the nanopore is a much more demanding task than the static background PL measurements: first, the former requires time synchronization between the pore blockade and the photon bursts and second, it involves consideration of additional sources of noise due to out-of-focus molecules. To evaluate the performance for opti-nanopore biopolymer detection, we produced two different ~1.9 kbp PCR amplicons and labeled them using either yellow or red fluorophores (dUTP-Atto550 or dUTP-Atto647N) by the nick translation method. Our labeling procedure and verification are shown in the Supporting Information, Figure S4. Based on UV–vis analysis we estimate that on average there are either 14 yellow or 10 red fluorophores per DNA molecule. The two labeled DNA molecules were mixed at equal molar concentration and subjected to analysis using a TiO_2 nanopore, as described in the methods section.

Figure 4b shows a representative concatenated series of electro-optical events. Our acquisition software analyzes the electrical signal in real-time and saves the corresponding signal buffers (synchronized electrical and optical) only if a translocation event is observed, by setting a current threshold at 0.85 of the open pore level. As shown in Figure 4b, DNA translocation produces *either* a green *or* red photon burst. The optical signal overlaps in time with the electrical signal (zoomed-in image shown in the figure insert). Furthermore, an analysis of a larger data set ($N = 90$) of yellow- or red-labeled DNA using 2D scatter plots shows a single pattern for the electrical events diagram (I_B *versus* t_D, left panel, Figure 4c) indicating that the two DNA molecules cannot be distinguished by the electrical signals due to their nearly identical lengths. However, the optical signals acquired from the same events, easily distinguishes the two differently labeled DNAs, as shown in the red versus green scatter plot (right panel).

Next, data analysis was performed off-line (see Methods) to evaluate the electrical/optical dwell times (t_D and t_O) based on individual thresholds levels. To circumvent the deviation of long dwell time to optical signal, the fluorescence intensity is defined

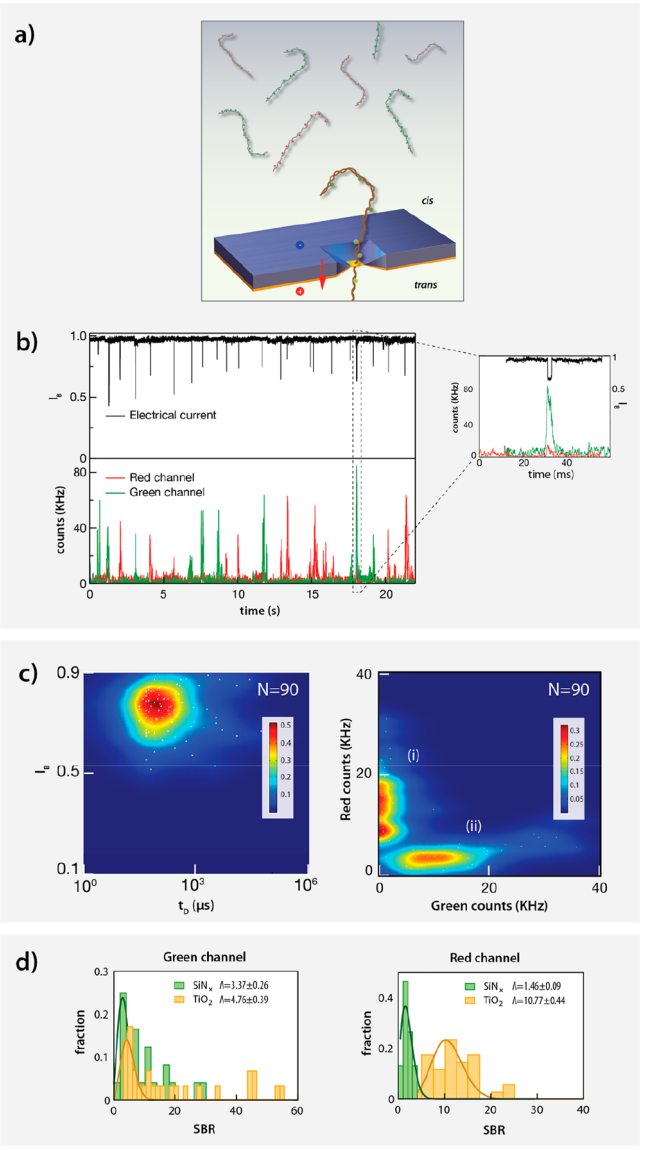

Figure 4. Two color electro-optical sensing of DNA translocation through TiO_2 nanopore, and SBR measurements. (a) Schematic representation of the two color electro-optical sensing. Two DNA samples, 1994 bp DNA labeled with Atto550, and 1827 bp DNA labeled with Atto647N, were added to the cis chamber at the concentration of 50 pM each. The two lasers (561 and 640 nm, P = 150 μW) were focused on the TiO_2 nanopore simultaneously. (b) Concatenated electro-optical events measured at 300 mV. Each electrical event (black line) was accompanied by an optical spike in the green or red channel. A close-up view of a representative electro-optical event is shown on the right. (c) Electrical and optical scatter plots. (Left panel) the electrical scatter plot showing only one population due to DNA length similarity (1827 bp and 1994 bp). (Right panel) the optical scatter plot of green channel versus red channel, presenting two distinct populations, allowing differentiation between the two DNA samples. (d) Optical SBR measurements using red or green labeled DNA translocations through SiN_x (green) and TiO_2 (yellow) nanopores in the green (left panel) and red (right panel) channels (Atto550-labeled 1994 bp dsDNA and Atto647N-labeled 1827 bp dsDNA, under 150 μW 561/640 nm laser illumination). Poisson fitting values are indicated in each case.

DOI: 10.1021/acsnano.8b07055
ACS Nano XXXX, XXX, XXX–XXX

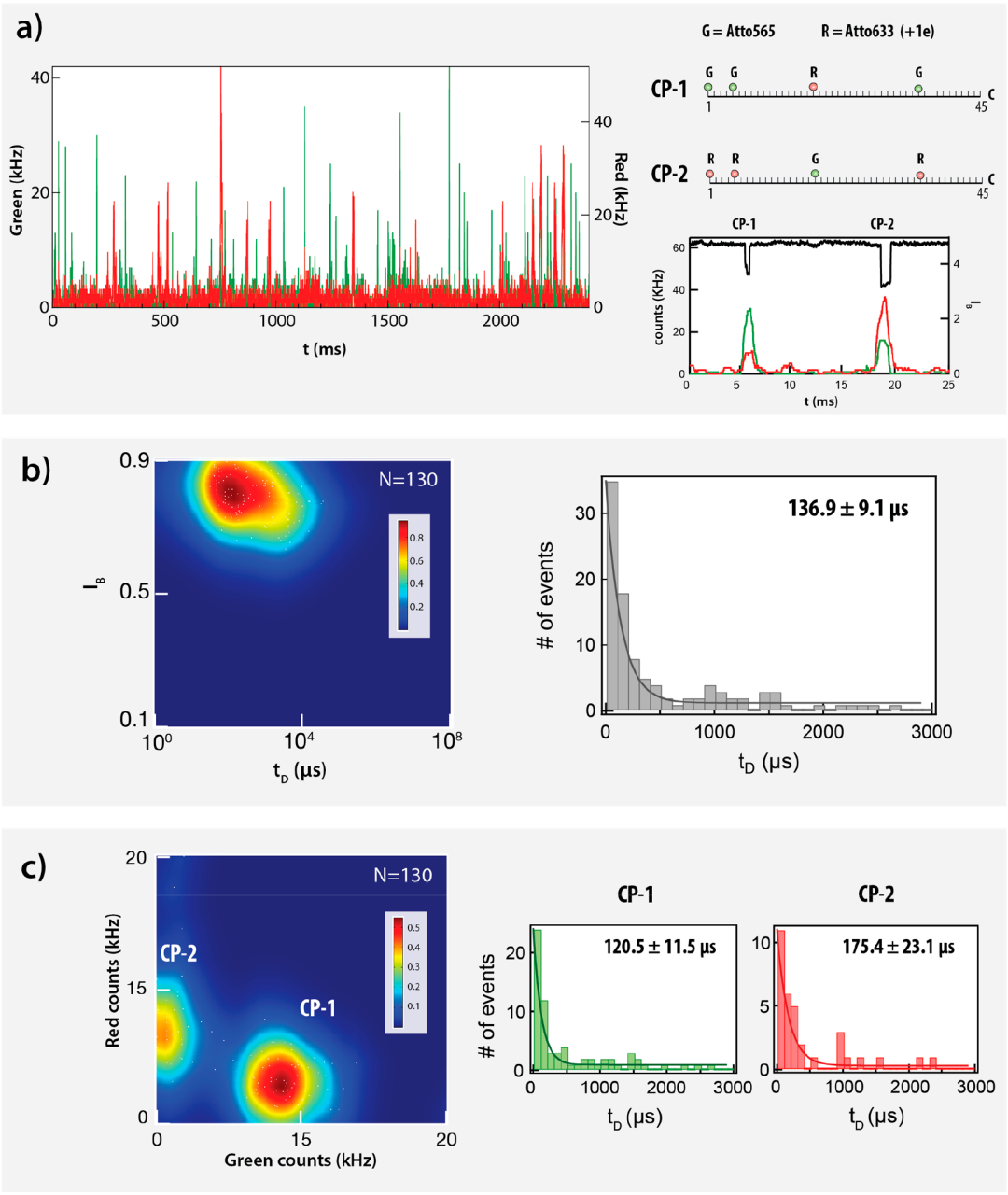

Figure 5. Real-time discrimination among labeled polypeptides is enabled due to the higher SBR in TiO_2 nanopores. (a) Concatenated events of optical peptide translocations at 300 mV under 500 μW 561/640 nm laser illuminations. Two identical 45 amino-acid peptides were labeled by either three green and one red fluorophores (Atto565 and Atto633, respectively) or by three red and one green fluorophores, as shown schematically. Inset shows two representative events of the primarily green (left) or red labeled peptide (right). (b) Electrical scatter plots. (Left panel) the electrical scatter-plot shows only one population. (Right panel) dwell time distribution shows one exponential decay with a time constant of 136.9 ± 9.1 μs. (c) Optical scatter plot of green channel versus red channel. (Left panel) the optical scatter-plot presents two distinct populations, allowing to differentiate between the labeled peptides. (Right panel) dwell time distribution for each population reveals slower translocation for the CP-2 peptide (175.4 ± 23.1 μs) as compared with the CP-1 peptide (120.5 ± 11.5 μs), resulting from the differences in their net charge due to the Atto633 dye, which adds a +1 charge upon conjugation.

as the total photon counts during electrical/optical dwell time divided by the electrical/optical dwell time. Figure S6 shows the histograms of the electrical and the optical dwell times. The time constant is calculated by tail fitting of the histogram by exponential function. Similar to our previous study, the optical dwell time (25.6 ± 2.4 ms) is much longer than the electrical dwell time (0.13 ± 0.01 ms).[23,40] This is expected, since the DNA macromolecule slowly diffuses in the vicinity of the pore and fluorophores are excited before and after its translocation.

TiO_2 Nanopores Have Higher SBR Compared to SiN_x Nanopores. To date, nanopore sensing of a single fluorophore during the passage of a labeled polypeptide has been challenging due to an insufficient SBR. As shown in Figure 3c, a laser intensity above ~100 μW would produce sufficient PL background in SiN_x membranes to completely inhibit single-fluorophore sensing (at this intensity, the expected single fluorophore signal is <10 kHz), while lower laser intensities would not produce sufficient photon fluxes for single-

DOI: 10.1021/acsnano.8b07055
ACS Nano XXXX, XXX, XXX−XXX

fluorophore sensing. Thus, to quantify the potential advantage of the TiO_2 nanopores in terms of their ultralow PL background, a detailed measurement of the SBR was performed with the above labeled dsDNA macromolecules. For each DNA translocation event, the total optical background was obtained by averaging the photon counts before and after optical dwell time. Then the optical signal was evaluated as the mean photon count during the optical dwell time minus the optical background. The ratio of the two numbers is defined as the SBR *during* each biomolecule's translocation. Figure 4d displays the SBR distributions calculated in the green and red channels (right and left panels, respectively) for the SiN_x or the TiO_2 nanopores (green and yellow bars, respectively). Solid lines represent Poisson fits expected for single-molecule fluorescence intensity histograms, with mean values indicated for each case. In the green channel, a mild increase in SBR of only ~40% is noted, whereas in the red channel, in which the PL of SiN_x is substantial, we observe about a 8-fold net increase in the SBR, and in some cases SBR > 20 are detected.

Polypeptides Discrimination Using High SBR TiO_2 Nanopores. The marked increase in SBR translates to better sensing resolution, and thus opens up additional opportunities for peptide detection. To demonstrate this enhanced sensing capability, we synthesized a 45 amino-acids long polypeptide harboring a *single* cysteine and *two* lysines residues for specific two-color labeling. This polypeptide was designed to lack secondary structures in aqueous solution and hence, with the appropriate adjustment of pH, this peptide linearly translocates through the nanopore. The polypeptide translocated through and was readily discernible using a 4 nm nanopore (see Supporting Information, Figure S8). Next we produced two variants of the same polypeptide (**CP-1** and **CP-2**) by coupling either three green fluorophores (Atto565 NHS-ester) to the three available primary amines in the molecule (the N-terminus and the two lysines) and a single red fluorophore (Atto633 maleimide) to a thiol group on the cysteine residue; or conversely three red fluorophores and a single green fluorophores on the polypeptide using the same chemistries (see Supporting Information Figure S7 and corresponding text for HPLC and MALDI data on peptide purity and composition, respectively). A schematic illustration of the two variants is shown in Figure 5a, right. As not limited by the high PL background of the SiN_x nanopores, we used the TiO_2 nanopores with an increased laser power of 500 μW. Notably, despite this high laser intensity, the optical background remains below ~1.5 kHz, allowing facile detection of single fluorophore during the passage of the CP-1 and CP-2 with SBR > 10. Moreover, it was readily possible to distinguish among the two peptide variants in real-time as shown in the concatenated representative event sets (Figure 5a left panel). The individual fluorophores (green or red) were resolved during the translocation of the peptide through the TiO_2 nanopore. Interestingly, we noticed that even though CP-1 and CP-2 have the same sequence, the dwell time of the CP-2 in the nanopore was slightly longer. This observation could be attributed to the difference in net charge in these two peptides as the Atto633 dye adds a +1 charge upon conjugation. Therefore, conjugation of the Atto633 reduces the overall negative charge of CP-2 from −9 to −7. The two populations could not be distinguished by the electrical signals (Figure 5b, left panel), or by the dwell times (Figure 5b, dwell time histograms right panel). However, the obtained optical signals allowed us to readily separate the events into two populations of higher green signals (representing CP-1) and higher red ones (representing CP-2). Analyzing each subpopulation separately revealed a slightly slower translocation for the CP-2 peptide (175.4 ± 23.1 μs) as compared with the CP-1 peptide (120.5 ± 11.5 μs), as expected.

CONCLUSIONS

A method for fabricating locally supported, free-standing, TiO_2 nanopore sensors is described. This wafer-scale fabrication method produces hundreds of highly robust TiO_2 devices at a relatively low cost. The TiO_2 chips exhibit comparable electrical noise and signals during DNA translocations to the widely used SiN_x nanopores. Importantly, PL measurements demonstrate that the TiO_2 membranes produce extremely low PL, even at relatively high laser intensities in both the green and the red wavelengths. This low level of PL is likely due to the inherently larger energy bandgap of the amorphous TiO_2 membrane as compared with the SiN_x membrane.

To highlight the advantages of these TiO_2 nanopore devices, we demonstrate both DNA and polypeptide discrimination based solely on the optical signals. The much-reduced PL background of the TiO_2 chips translates directly to a high SBR allowing for single fluorophore sensing, during the fast passage of a polypeptide through the nanopore. Importantly, this opens up the possibility of multicolor excitation including green, yellow, and red lasers, simultaneously. The ability to discriminate between two differently labeled, nearly identical-length, dsDNA molecules can be directly applied in single-molecule DNA methylation quantification involving multiple methyltransferase labeling enzymes,[23] each conjugating a specific color coded tag. Using site-specifically two-color labeled polypeptides, the high SBR allows identification of two variants of the same polypeptide, strictly by their labeling scheme. These results establish the basis for development of a protein characterization method based on the abundance and the location of specifically labeled amino acid residues (e.g., lysines and cysteines) within a peptide or protein,[25] which will be a subject of future studies.

METHODS

Free Standing TiO_2 Membranes and Nanopores Fabrication. Chips were fabricated from a double-sided polished Si wafer coated with 500 nm thermal SiO_2, on which 50 nm low-stress SiN_x layer was deposited using low pressure chemical vapor deposition (LPCVD, Cornell CNF). The fabrication included the following steps: first, a thinner region is formed at the SiN_x by either *e*-beam or direct-write photolithography (MicroWriter ML3, DMO), followed by selective etching of the circles pattern using reactive ion etch (RIE, Diener Electronic). Next, the wafer was cleaned thoroughly, and atomic-layer deposition (ALD, GEMStar XT, Arradiance) was used to deposit TiO_2 with required thickness on both sides of the wafer. Then photolithography was used again to form the hard-mask for KOH wet etch of the Si. To remove the thin layer of SiN_x left in the thin region after the KOH etch, RIE etching was applied on the back side, taking advantage of the fact that SiN_x etch rate is at least 10 times faster than the TiO_2 (see Figure S1 and S2 in the Supporting Information for detailed chip fabrication description). Finally, a nanopore was drilled in the TiO_2 thin region using either controlled dielectric breakdown (CDB), or high-resolution transmission electron microscopy (TEM). For CDB we used the voltage-pulsed strategy as described before.[34] Pulses of 6 V (60 ms long) were applied on the membrane. Current jump, indicating pore formation, was observed in less than 10 min.

Electro-Optical Setup. The electro-optical measurement system consists of two parts: (1) Confocal microscopy to detect optical signals. A high NA objective is used to focus 3 collimated, expanded lasers (532, 561, and 640 nm, iFlex-Viper) on the nanopore, as well as to collect the

DOI: 10.1021/acsnano.8b07055
ACS Nano XXXX, XXX, XXX−XXX

emitted light. After passing through the appropriate filters and a pinhole, the emitted light is split (cutoff wavelength of 650 nm) and recorded by two APDs; (2) The ionic current is measured by immersing two Ag/AgCl electrodes into the cis and the trans chambers, linked to an Axon Axopatch 200B patch-clamp amplifier filtered at 10 kHz. The optical signals and analogue electrical signals are obtained using National Instruments NI-6602 and NI-6154 DAQ cards, respectively. The two acquisition cards were synchronized *via* a hardware connection and fully controlled using a custom LabVIEW program. For the Ca^{2+} activators based imaging of the pore we used wide field illumination of the membrane using a 488 nm laser as described by Zrehen *et al.*[34]

Experimental Flow. Chips were cleaned by acetone, methanol, isopropyl alcohol and deionized water, followed by oxygen plasma or UV/ozone treatment. The chips were then mounted on a homemade PTFE cell using fast-curing PMDS. Nanopores were drilled by CDB after filling the two chambers with 1 M KCl buffer containing 40 mM Tris, and 1 mM EDTA, pH 8. The DNA and peptides translocation experiments were conducted using the same buffer. The labeled biomolecules were added to the cis chamber, facing the front side of the membrane. The electrical events were recorded under 200, 300, and 400 mV at the concentration of 0.5 nM. For the optical sensing, the nanochip PTFE cell was mounted on a XYZ nanopositioner stage (Physik Instrumente) above the objective. Translocation events were measured under a bias of 300 mV at the concentration of 0.1 nM. Yellow (561 nm) and red (640 nm) lasers were focused on the pore with intensity of 150 μW each for DNA sensing, and 500 μW for the peptides. Simultaneous electrical and optical events were detected, indicating that the CDB-drilled nanopore was located exactly in the thin region of the membrane, in agreement with the calcium indicator experiment.

Data Analysis. An offline LabVIEW program was used to analyze each event separately by two consecutive steps: (i) An electrical threshold was applied on the electrical trace to extract the dwell time (t_D), and the amplitude drop ($I_B = i_B/i_O$) of the event. (ii) An optical threshold was then applied on the optical signals, detected at the same period of time, to extract the optical dwell time, the optical background in each channel, and the photon flux in each channel during the optical event (I_{Opt_ch1}, I_{Opt_ch2}). The calculated values of the electrical and the optical parameters were then used to create histograms of each parameter or a heat map of t_D vs I_B and I_{Opt_ch1} vs I_{Opt_ch2}. The photon flux during the event and the background were used to estimate the optical signal to background ratio (SBR) in each channel for each event.

Sample Preparation. A 1994 bp DNA fragment was amplified from a 5000 bp NoLimits DNA (Thermo Fisher Scientific), and a 1827 bp DNA fragment was amplified from CDKN2A gene in genomic DNA using PCR. The 1994 bp DNA and 1827 bp DNA samples were purified using the PCR cleanup kit (Macherey-Nagel), and labeled using Nick Translation with Aminoallyl-dUTP-Atto550 (Sigma) and Aminoallyl-dUTP-Atto647N (Sigma), respectively. Finally, the labeled samples were purified by QIAQuick PCR cleanup kit (Qiagen) and ethanol precipitation.

Synthetic peptides were purchased from Genscript (Piscataway, NJ, USA), and dissolved in the reaction buffer at a concentration of 1 mg/mL. The peptides were labeled using two labeling reactions. Malemide dyes (ATTO633/565 GmbH, Germany) were first used to label the thiol groups on the cysteines. The amine groups on the peptide (the N-terminus and two lysines residues) were then labeled with NHS ester dyes (ATTO565/633 GmbH, Germany). Each labeling step was followed by purification using gel filtration chromatography (GE Healthcare, USA). Detailed sample preparation description of the dsDNA and the peptides as well as their sequences, are provided in the Supporting Information.

ASSOCIATED CONTENT

Supporting Information

The Supporting Information is available free of charge on the ACS Publications website at DOI: 10.1021/acsnano.8b07055.

Wafer-scale fabrication of TiO_2 nanopore sensors, wafer-scale fabrication of SiN_x nanopore sensors, electro-optical setup, PL intensity comparison between SiN_x and TiO_2 membranes, preparation of 5054 bp double stranded DNA for electrical characterization, preparation of dUTP-Atto550 or Atto647N labeled DNA fragments, translocation dwell time histograms of the dsDNA molecules, peptide labeling and purification (CP633565), characterization of peptides' translocation through a SiN_x nanopore (PDF)

AUTHOR INFORMATION

Corresponding Authors

*E-mail: mgrin@bu.edu.
*E-mail: ameller@technion.ac.il.

ORCID

Mark W. Grinstaff: 0000-0002-5453-3668
Amit Meller: 0000-0001-7082-0985

Author Contributions

#R.W. and T.G. contributed equally.

Notes

The authors declare no competing financial interest.

ACKNOWLEDGMENTS

We acknowledge financial support from the BeyondSeq consortium (EC program 63489 to A.M) and i-Core program of the Israel Science Foundation (1902/12 to A.M.).

REFERENCES

(1) Dekker, C. Solid-State Nanopores. *Nat. Nanotechnol.* **2007**, *2*, 209−215.
(2) Wanunu, M.; Meller, A. Single-Molecule Analysis of Nucleic Acids and DNA−Protein Interactions Using Nanopores. In *Laboratory Manual on Single Molecules*; Ha, T., Selvin, P., Eds.; Cold Spring Harbor Press: 2008, p 507.
(3) Wanunu, M.; Dadosh, T.; Ray, V.; Jin, J.; McReynolds, L.; Drndic, M. Rapid Electronic Detection of Probe-Specific MicroRNAs Using Thin Nanopore Sensors. *Nat. Nanotechnol.* **2010**, *5*, 807−814.
(4) Meller, A.; Nivon, L.; Branton, D. Voltage-Driven DNA Translocations through a Nanopore. *Phys. Rev. Lett.* **2001**, *86*, 3435−3438.
(5) Singer, A.; Rapireddy, S.; Ly, D. H.; Meller, A. Electronic Barcoding of a Viral Gene at the Single-Molecule Level. *Nano Lett.* **2012**, *12*, 1722−1728.
(6) Squires, A. H.; Atas, E.; Meller, A. Genomic Pathogen Typing Using Solid-State Nanopores. *PLoS One* **2015**, *10*, e0142944.
(7) Squires, A.; Atas, E.; Meller, A. Nanopore Sensing of Individual Transcription Factors Bound to DNA. *Sci. Rep.* **2015**, *5*, 1−11.
(8) Atas, E.; Singer, A.; Meller, A. DNA Sequencing and Bar-Coding Using Solid-State Nanopores. *Electrophoresis* **2012**, *33*, 3437−3447.
(9) Wanunu, M. Nanopores: A Journey Towards DNA Sequencing. *Phys. Life Rev.* **2012**, *9*, 125−158.
(10) Feng, J.; Liu, K.; Bulushev, R. D.; Khlybov, S.; Dumcenco, D.; Kis, A.; Radenovic, A. Identification of Single Nucleotides in MoS_2 Nanopores. *Nat. Nanotechnol.* **2015**, *10*, 1070−1076.
(11) Bayley, H. Nanopore Sequencing: From Imagination to Reality. *Clin. Chem.* **2015**, *61*, 25−31.
(12) Yusko, E. C.; Johnson, J. M.; Majd, S.; Prangkio, P.; Rollings, R. C.; Li, J.; Yang, J.; Mayer, M. Controlling Protein Translocation through Nanopores with Bio-inspired Fluid Walls. *Nat. Nanotechnol.* **2011**, *6*, 253−260.
(13) Rotem, D.; Jayasinghe, L.; Salichou, M.; Bayley, H. Protein Detection by Nanopores Equipped with Aptamers. *J. Am. Chem. Soc.* **2012**, *134*, 2781−2787.
(14) Plesa, C.; Kowalczyk, S. W.; Zinsmeester, R.; Grosberg, A. Y.; Rabin, Y.; Dekker, C. Fast Translocation of Proteins through Solid State Nanopores. *Nano Lett.* **2013**, *13*, 658−663.

DOI: 10.1021/acsnano.8b07055
ACS Nano XXXX, XXX, XXX−XXX

(15) Nir, I.; Huttner, D.; Meller, A. Direct Sensing and Discrimination among Ubiquitin and Ubiquitin Chains Using Solid-State Nanopores. *Biophys. J.* **2015**, *108*, 2340−2349.
(16) Restrepo-Pérez, L.; John, S.; Aksimentiev, A.; Joo, C.; Dekker, C. SDS-assisted Protein Transport through Solid-State Nanopores. *Nanoscale* **2017**, *9*, 11685−11693.
(17) Varongchayakul, N.; Huttner, D.; Grinstaff, M. W.; Meller, A. Sensing Native Protein Solution Structures Using a Solid-State Nanopore: Unraveling the States of VEGF. *Sci. Rep.* **2018**, *8*, 1017.
(18) Traversi, F.; Raillon, C.; Benameur, S. M.; Liu, K.; Khlybov, S.; Tosun, M.; Krasnozhon, D.; Kis, A.; Radenovic, A. Detecting the Translocation of DNA through a Nanopore Using Graphene Nanoribbons. *Nat. Nanotechnol.* **2013**, *8*, 939−945.
(19) Puster, M.; Balan, A.; Rodríguez-Manzo, J. A.; Danda, G.; Ahn, J. H.; Parkin, W.; Drndić, M. Cross-Talk Between Ionic and Nanoribbon Current Signals in Graphene Nanoribbon-Nanopore Sensors for Single-Molecule Detection. *Small* **2015**, *11*, 6309−6316.
(20) McNally, B.; Singer, A.; Yu, Z.; Sun, Y.; Weng, Z.; Meller, A. Optical Recognition of Converted DNA Nucleotides for Single-Molecule DNA Sequencing Using Nanopore Arrays. *Nano Lett.* **2010**, *10*, 2237−2244.
(21) Assad, O. N.; Di Fiori, N.; Squires, A. H.; Meller, A. Two Color DNA Barcode Detection in Photoluminescence Suppressed Silicon Nitride Nanopores. *Nano Lett.* **2015**, *15*, 745−752.
(22) Sawafta, F.; Clancy, B.; Carlsen, A. T.; Huber, M.; Hall, A. R. Solid-State Nanopores and Nanopore Arrays Optimized for Optical Detection. *Nanoscale* **2014**, *6*, 6991−6996.
(23) Gilboa, T.; Torfstein, C.; Juhasz, M.; Grunwald, A.; Ebenstein, Y.; Weinhold, E.; Meller, A. Single-Molecule DNA Methylation Quantification Using Electro-optical Sensing in Solid-State Nanopores. *ACS Nano* **2016**, *10*, 8861−8870.
(24) Zhang, M.; Ngampeerapong, C.; Redin, D.; Ahmadian, A.; Sychugov, I.; Linnros, J. Thermophoresis-Controlled Size-Dependent DNA Translocation through an Array of Nanopores. *ACS Nano* **2018**, *12*, 4574−4582.
(25) Yao, Y.; Docter, M.; van Ginkel, J.; de Ridder, D.; Joo, C. Single-Molecule Protein Sequencing through Fingerprinting: Computational Assessment. *Phys. Biol.* **2015**, *12*, 055003.
(26) Restrepo-Pérez, L.; Joo, C.; Dekker, C. Paving the Way to Single-Molecule Protein Sequencing. *Nat. Nanotechnol.* **2018**, *13*, 786−796.
(27) Dette, C.; Pérez-Osorio, M. A.; Kley, C. S.; Punke, P.; Patrick, C. E.; Jacobson, P.; Giustino, F.; Jung, S. J.; Kern, K. TiO_2 Anatase with a Bandgap in the Visible Region. *Nano Lett.* **2014**, *14*, 6533−6538.
(28) Schneider, J.; Matsuoka, M.; Takeuchi, M.; Zhang, J.; Horiuchi, Y.; Anpo, M.; Bahnemann, D. W. Understanding TiO_2 Photocatalysis: Mechanisms and Materials. *Chem. Rev.* **2014**, *114*, 9919−9986.
(29) Tang, H.; Prasad, K.; Sanjinès, R.; Schmid, P. E.; Lévy, F. Electrical and Optical Properties of TiO_2 Anatase Thin Films. *J. Appl. Phys.* **1994**, *75*, 2042−2047.
(30) Merchant, C. A.; Healy, K.; Wanunu, M.; Ray, V.; Peterman, N.; Bartel, J.; Fischbein, M. D.; Venta, K.; Luo, Z.; Johnson, A. T. C.; Drndić, M.; Drndić, M. DNA Translocation through Graphene Nanopores. *Nano Lett.* **2010**, *10*, 2915−2921.
(31) dela Torre, R.; Larkin, J.; Singer, A.; Meller, A. Fabrication and Characterization of Solid-State Nanopore Arrays for High-Throughput DNA Sequencing. *Nanotechnology* **2012**, *23*, 385308.
(32) Storm, A. J.; Chen, J. H.; Ling, X. S.; Zandbergen, H. W.; Dekker, C. Fabrication of Solid-State Nanopores with Single-Nanometre Precision. *Nat. Mater.* **2003**, *2*, 537−540.
(33) Kim, M. J.; Wanunu, M.; Bell, D. C.; Meller, A. Rapid Fabrication of Uniformly Sized Nanopores and Nanopore Arrays for Parallel DNA Analysis. *Adv. Mater.* **2006**, *18*, 3149−3153.
(34) Zrehen, A.; Gilboa, T.; Meller, A. Real-Time Visualization and Sub-Diffraction Limit Localization of Nanometer-Scale Pore Formation by Dielectric Breakdown. *Nanoscale* **2017**, *9*, 16437−16445.
(35) Kowalczyk, S. W.; Grosberg, A. Y.; Rabin, Y.; Dekker, C. Modeling the Conductance and DNA Blockade of Solid-State Nanopores. *Nanotechnology* **2011**, *22*, 315101.
(36) Tabard-Cossa, V.; Trivedi, D.; Wiggin, M.; Jetha, N. N.; Marziali, A. Noise Analysis and Reduction in Solid-State Nanopores. *Nanotechnology* **2007**, *18*, 305505.
(37) Anderson, B. N.; Assad, O. N.; Gilboa, T.; Squires, A. H.; Bar, D.; Meller, A. Probing Solid-State Nanopores with Light for the Detection of Unlabeled Analytes. *ACS Nano* **2014**, *8*, 11836−11845.
(38) Wanunu, M.; Sutin, J.; McNally, B.; Chow, A.; Meller, A. DNA Translocation Governed by Interactions with Solid-State Nanopores. *Biophys. J.* **2008**, *95*, 4716−4725.
(39) Akahori, R.; Haga, T.; Hatano, T.; Yanagi, I.; Ohura, T.; Hamamura, H.; Iwasaki, T.; Yokoi, T.; Anazawa, T. Slowing Single-Stranded DNA Translocation through a Solid-State Nanopore by Decreasing the Nanopore Diameter. *Nanotechnology* **2014**, *25*, 275501.
(40) Assad, O. N.; Gilboa, T.; Spitzberg, J.; Juhasz, M.; Weinhold, E.; Meller, A. Light-Enhancing Plasmonic-Nanopore Biosensor for Superior Single-Molecule Detection. *Adv. Mater.* **2017**, *29*, 1605442−9.

DOI: 10.1021/acsnano.8b07055
ACS Nano XXXX, XXX, XXX−XXX